JOURNAL OF THERMOPHYSICS AND HEAT TRANSFER
Vol. 20, No. 4, October–December 2006

Comparison of Enthalpy Determination Methods for Arc-Jet Facility

Chul Park*
Eloret Corporation, Sunnyvale, California 94035
and
George A. Raiche, II,† David M. Driver,† Joseph Olejniczak,†
Imelda Terrazas-Salinas,‡ T. Mark Hightower,‡ and Takeharu Sakai§
NASA Ames Research Center, Moffett Field, California 94035

Four experimental methods of determining the enthalpy of the flow in an arc-jet facility that is, the heat balance method, the sonic throat method, the heat transfer method, and the emission-spectroscopic method, are compared with a computational fluid dynamics (CFD) solution. The comparison is made for the Interaction Heating Facility of NASA Ames Research Center for one operating condition. The mass-averaged enthalpy values determined by the heat-balance method and the sonic throat method are 28.7 and 28.8 MJ/kg, respectively. The lower bound of the centerline enthalpy value determined by the heat transfer rate method is 30.5 MJ/kg. The spectrometric method resulted in the centerline enthalpy value of 40.6 MJ/kg. The CFD solution yields the centerline and the average enthalpy values at the nozzle throat of 41.0 and 27.0 MJ/kg, respectively.

Nomenclature

A	=	cross-sectional area of the nozzle throat, m^2
D	=	model base diameter, m
d	=	distance from model wall, mm
$F(\lambda, r)$	=	Radial viewing function, Eq. (3)
$f(\lambda, r)$	=	Lateral viewing function, Eq. (4)
H_{av}	=	mass-averaged enthalpy, J/kg
H_c	=	centerline enthalpy, J/kg
$\dot{m}$	=	mass flow rate, kg/s
p	=	pressure, Pa
q	=	stagnation-point heat transfer rate, W/m^2
R	=	equivalent nose radius, m
r	=	radial distance, Fig. 7
T	=	temperature, K
U	=	flow velocity, m/s
x	=	horizontal distance, Fig. 7
y	=	vertical distance, Fig. 7
γ	=	surface–catalytic recombination coefficient
λ	=	wavelength, nm

Subscripts

A	=	argon
a	=	air
e	=	electron
v	=	vibration
0	=	settling chamber

Presented as Paper 2004-0487 at the 42nd Aerospace Sciences Meeting, Reno, NV, 5–8 January 2004; received 26 September 2005; revision received 16 December 2005; accepted for publication 22 January 2006.

*Senior Research Scientist; currently Professor, Department of Aerospace Engineering, Korea Advanced Institute of Science and Technology, 373-1 Guseong-dong, Yuseong-gu, Daejeon, Republic of Korea 305-701; cpark216@kaist.ac.kr. Fellow AIAA.

†Research Scientist, Reacting Flow Environments Branch. Member AIAA.

‡Research Scientist, Thermophysics Facilities Branch. Member AIAA.

§National Research Council Research Associate, Reacting Flow Environments Branch. Member AIAA.

Introduction

ARC-JET facilities are used to produce the heating environment of high-speed planetary entry flights. One important parameter that such tests must simulate is the flow enthalpy. In the test section of an arc-jet facility, enthalpy is the highest at the centerline, decreases gradually toward the wall in the inner region, and decreases rapidly in the outer region near the wall. The inner region of the test-section stream in which flow properties vary slowly is called the core region, and tests are made within this region. The enthalpy of this core region is referred to commonly as the centerline or core enthalpy. It is this centerline enthalpy that must simulate the flight value. In contrast, the mass average of the enthalpy in the stream, including the portion in the cold outer region, is called the mass-averaged enthalpy. The ratio of the centerline enthalpy to the mass-averaged enthalpy, which is by definition greater than unity, is an important parameter in the use of the arc-jet facilities. Because heat transfer rate is proportional to enthalpy, any uncertainty in this value translates directly to the uncertainty in the performance of the tested heatshield material.

The mass-averaged enthalpy can be determined experimentally relatively simply in two different ways: 1) by dividing the net power input by the mass flow rate in a so-called heat balance method and 2) from the relationship between the enthalpy and the flow rate in a method called the sonic throat method. The centerline enthalpy can also be determined in two different ways: 1) from the heat transfer rate to the stagnation point of a blunt body in a method known as heat transfer method and 2) by analyzing the spectrum of the radiation emitted by the shock layer, that is, the spectrometric method. The last two methods are more difficult to carry out than the first two. In addition, the laser-induced fluorescence (LIF) method promises to determine the thermodynamic state of the test-section flow completely, including the flow enthalpy.[1] However, presently, this method is not advanced sufficiently to be able to measure all components of energy including those in the internal modes.

Determining these enthalpy values entirely theoretically was not possible until recently. Very recently, computational fluid dynamic (CFD) calculation of the arc-jet flows, which is entirely theoretical, became possible.

Despite the importance of the accuracy of the enthalpy value, no systematic comparison has been made to date among the methods just mentioned. In the present work, the currently possible four experimental methods are applied to one operational condition of an arc-jet facility, the Interaction Heating Facility (IHF) at NASA Ames Research Center. The IHF operates on a maximum steady electrical power input of 60 MW and is sometimes referred to as the 60-MW

facility. The enthalpy values thus determined are compared with the solution of a CFD calculation. When efforts are concentrated on one operating condition, statistical smapling needed in assessing reproducibility is obtained. It is hoped that the findings of this work will lead to a similar effort over a wider range of operating conditions.

Facility Operating Conditions

The IHF has a segmented constrictor 8 cm in diameter and 3.97 m in length. The throat diameter is 6.03 cm. For the tests analyzed in the present work, the nozzle was conical with a cone half-angle of 10 deg and had an exit diameter of 15.2 cm, resulting in a geometrical area ratio of 6.35.

Dry air is used as the main test gas. The flow rate of air was nominally 0.38 kg/s. Argon was added at a nominal flow rate of 0.031 kg/s. The data taken in 25 separate runs were analyzed in the present work. Throughout these tests, the electrical current was maintained at an average value of 6066 A. The standard (root mean square) deviation in the current was 58.6 A. The voltage between the electrodes was 4828 V, with a standard deviation of 34.1 V, resulting in an average electrical power input of 29.3 MW. The standard deviation in the power input was 0.28 MW. The total flow rate was 0.412 kg/s with a standard deviation of 0.33%. The pressure in the settling chamber p_0 was 0.453 MPa, with a standard deviation of 2.7 kPa.

All measurements were made at approximately 11 cm downstream of the exit plane of the nozzle. The distance from the nozzle throat to the model position was 0.4 m. Pitot pressure was measured in 13 of the 25 tests. The average value and the standard deviation of the pitot pressure were 65.8 and 0.31 kPa, respectively.

To investigate the influence of flow enthalpy on spectral characteristics of the radiation emitted by the shock layer, calculation was performed for the nozzle for four different assumed values of settling chamber enthalpy: 32, 39, 44.5, and 47.3 MJ/kg. An improved version of the one-dimensional nozzle flow code NOZNT described in Ref. 2 was used for this purpose. In this code, six different temperatures are accounted for: heavy particle translational–rotational temperature; vibrational temperatures of O_2, N_2, and NO; electron temperature T_e; and electronic temperature $T_{\text{electronic}}$. The electronic temperature is the temperature that characterizes the electronic excitation energy of the gas atoms and molecules. The six-temperature calculation showed that the test-section flow consisted mostly of atomic oxygen and molecular nitrogen and that electron temperature, electronic temperature, and vibrational temperature of N_2 are almost equal. This implies that a two-temperature description, one temperatue for the translational–rotational mode and the other temperature for the N_2 vibrational, electron, and electronic mode, would be sufficient to describe the relaxation behavior behind the bow shock in the test section.

Three different sets of reaction rate coefficients were considered in this study: the set given in Ref. 3, which is referred to hereafter as the standard rate set; the rates 1/10 thereof; and the rates 10 times thereof. The factors of 1/10 and 10 are believed to be the limit of uncertainty of the rate coefficient values involved.

In the calculation of the nozzle flow, the nozzle is described by a combination of two smooth hyperbolas to generate a slightly bell-jar shaped geometry. The effective nozzle area ratio at the location of the model is determined from the measured pitot pressure to be 10. The assumed nozzle profile produces an area ratio of two at the distance of 0.133 m from the throat.

The result obtained for the case of settling chamber enthalpy of 44.5 MJ/kg with the standard rate coefficients is shown in Table 1. This particular solution will be called the reference condition because, as will be shown later, this condition is consistent with the spectroscopic data obtained.

According to Table 1, the concentration of nitrogen atoms is more than three times that of oxygen atoms. The concentration of molecular oxygen is small. Because the bow shock wave over a blunt body heats the flow, the concentration of nitrogen molecules will be even lower in the shock layer. The convective heat transfer rate to a body placed in the test section will be affected greatly by the possible surface catalytic recombination of oxygen and nitrogen atoms. The intensity of radiation by nitrogen molecules will be relatively small compared with those from oxygen and nitrogen atoms. Though not shown, this feature holds true even with the reaction rates 0.1 or 10 times the standard values.

Table 1 Reference nozzle flow conditions calculated with standard rate coefficients[2]

Quantity	Settling chamber	Test section
Enthalpy, MJ/kg	44.5	40.6[a]
Pressure, Pa	4.700^{5}	2.517^{3}
Density, kg/m^3	8.177^{-2}	1.968^{-3}
Velocity, m/s	0	5890
Temperature, K		
Heavy particle	10,443	2594
T_v of O_2	10,443	3137
T_v of N_2	10,443	5577
T_v of NO	10,443	2598
T_e	10,443	3356
$T_{\text{electronic}}$	10,443	6564
Species mole fractions		
O	2.019^{-1}	2.161^{-1}
N	7.387^{-1}	6.871^{-1}
A	2.875^{-2}	3.041^{-2}
O_2	0	5.579^{-6}
N_2	7.563^{-3}	6.413^{-2}
NO	4.072^{-4}	4.924^{-6}
O^+	1.656^{-3}	8.086^{-4}
N^+	9.631^{-3}	3.601^{-4}
NO^+	1.189^{-4}	1.867^{-8}
Pitot pressure, Pa	NA	6.791^{4}

[a]Enthalpy as evaluated by two-temperature model using N_2 vibrational temperature; see text.

Note that even though the nozzle flow properties are calculated using the six-temperature model, the calculations of the shock-layer flow are made using the more widely used two-temperature model. When the vibrational temperature of N_2 is used as the vibrational–electron–electronic temperature in the two-temperature model, the enthalpy value in the freestream in the test section is calculated to be 40.6 MJ/kg for this case as presented in Table 1. The discrepancy between the settling chamber enthalpy of 44.5 MJ/kg and the freestream enthalpy of 40.6 MJ/kg is attributed to the electronic excitation energy in the freestream not accounted for in the two-temperature model. In reality, the true electronic temperature is unknown because radiative energy loss, which preferentially removes the electronic excitation energy in the nozzle, is unknown.

Mass-Averaged Enthalpy Measurement

Heat Balance Method

The average enthalpy of the flow produced by the facility can be determined experimentally using the heat balance method. In this method, the average enthalpy is determined by dividing the total power input into the flow by the mass flow rate of the test gas. The total power input is the electrical power input minus the cooling water loss.

At the time of the present series of experiment, the instrumentation necessary for the heat balance method was not functioning. Subsequently, the necessary instrumentation was installed. The instrumentation consisted of measuring the water flow rate by an ultrasound sensor and measuring the water temperature with a resistance-type detector strapped to the outside wall of the water passage.[4] The temperature detector is placed at a middle of a long tube that is at a nearly constant temperature, and, therefore, heat conduction out of the measuring region occurs only through the quiescent air surrounding the detector, which is believed to be small. One run was made in which the electrical current and voltage and the air mass flow rate were the same as in the test series of consideration. Additionally, air flow was introduced in the settling chamber to an amount equivalent to 12% of the flow through the constrictor. The addition of airflow in the settling chamber is not expected to affect the arc heater efficiency. The measured arc heater efficiency was 0.403.

When the efficiency value of 0.403 is used, the mass-averaged enthalpy in the present test series is determined to be 28.7 MJ/kg, with a standard deviation of 0.28 MJ/kg.

Sonic Throat Method

The sonic throat method relies on the principle that the flow is choked at the nozzle throat. For an inviscid equilibrium flow of air, the relationship between the flow rate through the throat $\dot{m}$ and the flow enthalpy H has been derived in Ref. 5 as

$$H = (0.293Ap_0/\dot{m})^{2.519} \tag{1}$$

A slightly different procedure is proposed in Ref. 6, in which the relationship between the mass-averaged enthalpy and the flow rate at the exit of the constrictor is utilized. Reference 6 shows that, in the range of enthalpy of most interest, this method produces a mass-averaged enthalpy value that is nearly the same as that by Eq. (1). Therefore, Eq. (1) is used in the present work to determine the mass-averaged enthalpy.

There were a total of 23 runs from which the needed information was gathered in the present test series. The average enthalpy value calculated from these 23 runs was 28.83 MJ/kg, with an standard deviation of 0.53 MJ/kg.

Centerline Enthalpy Measurement

Heat Transfer Method

The heat transfer rate at the stagnation point of a blunt axisymmetric body placed at the centerline of the test section is a function only of the properties along the centerline of the test flow. The functional relationship between the centerline flow properties and the heat transfer rate is well known. (The presence of argon in the flow was accounted for in deducing enthalpy from the measured heat transfer rate.) Using this relationship, one could deduce the centerline enthalpy from the measured stagnation-point heat transfer rate. To do so, however, one needs to know the catalytic efficiency of the wall to the recombination of oxygen and nitrogen atoms, and herein lies the uncertainty of the method.

To carry out the measurement of the stagnation-point heat transfer rate in the absence of ablation in the present work, that is, the so-called cold-wall stagnation-point heating rate, two copper slug calorimeters of a rounded flat disk shape, one with an overall diameter D of 2.54 cm and the other of 5.08 cm, were used. They are shown schematically in Fig. 1. As shown, the thermocouple junction is on the backface of the copper slug. The edge of these models are rounded as shown in Fig. 1. The ratio of the edge radius to the base radius was kept at 0.1875. The surface of the copper slug was polished before each test. The response of this gauge had been tested earlier against seveal different types of heat transfer gauges to verify its accuracy in the common operating range.

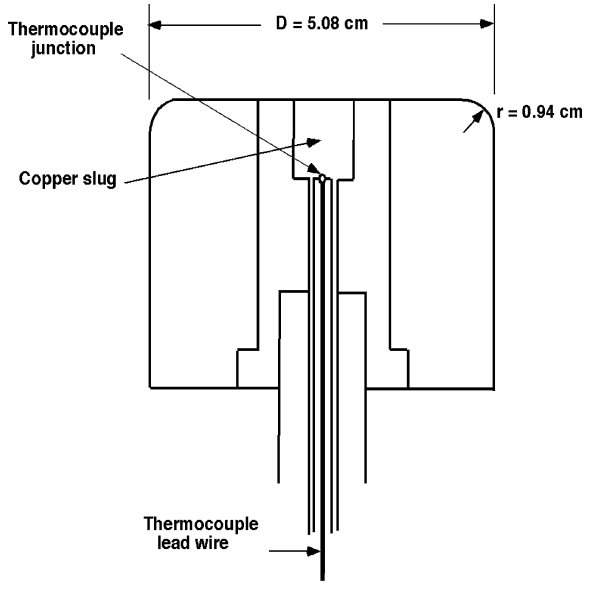

Fig. 1 Schematic of copper slug calorimeter heat transfer gauge.

In Fig. 2, a typical output of the thermocouple on the copper calorimeter is shown. A best-fit curve is drawn through the measured temperature values, and the heating rate is determined from it.

When the results of the heat transfer measurement are deduced, radiation is neglected: A separate calculation showed that the radiative heat transfer is only about 1% of the convective heating rate in the tested environment.

According to Ref. 7, the stagnation-point heating rate to the body of this shape is the same as that of a sphere with a radius R 3.15 times the base radius, or $R = 4.0$ cm for the $D = 2.54$ cm model and $R = 8.0$ cm for the $D = 5.08$ cm model.

The measured heat transfer values q are presented in Fig. 3, and are compared with the theoretical values. For the $D = 2.54$ cm model, five experimental points were obtained, with the average and the standard deviation of 1566.4 and 56.3 W/cm^2 (3.6%), respectively. For the $D = 5.08$ cm model, they were 1104.8 and 45.1 W/cm^2 (4.1%), respectively.

In Fig. 3, two sets of theoretical values are shown: the equilibrium value, known also as the Fay–Riddell value,[8] and the frozen value

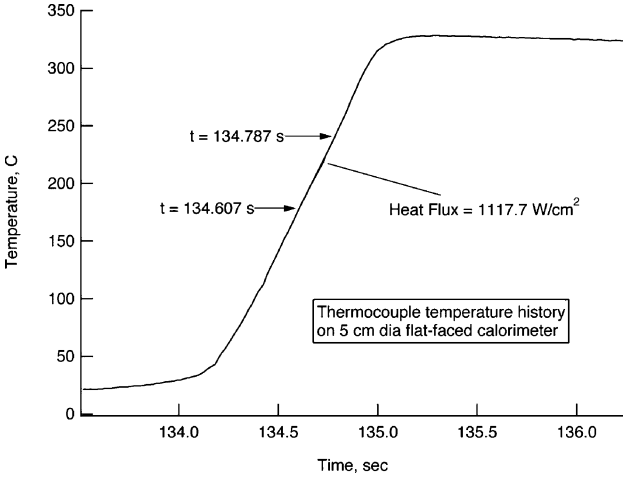

Fig. 2 Typical output from copper slug calorimeter.

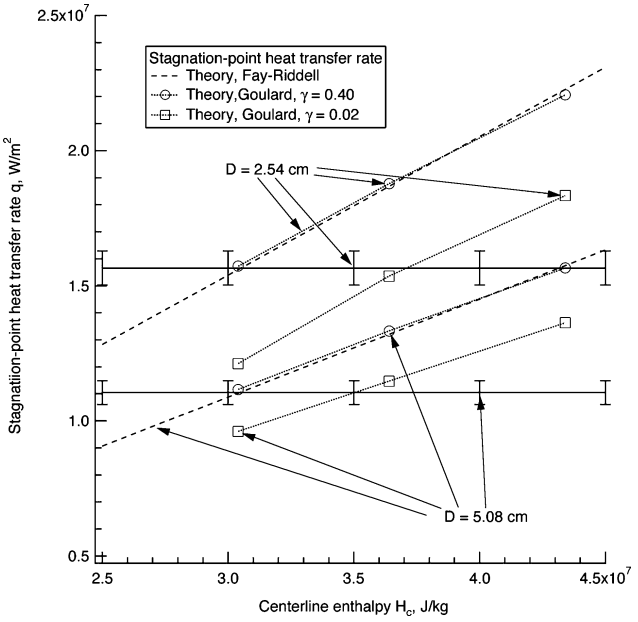

Fig. 3 Comparison between measured and calculated stagnation-point heat transfer rates.

calculated by the formula by Goulard.[9] The Fay–Riddell values are calculated using the formula given in Ref. 10,

$$H_c = q/\dot{m}\sqrt{R/p_0}(\dot{m}_A/K_A + \dot{m}_a/K_a) \quad (2)$$

in joules per kilogram, where the constants K_a and K_A are 3.905×10^{-4} and 5.513×10^{-4}, respectively. The heat transfer rate q is expressed in watts per square meter, R in meters, and p in pascal. This formula leads to the enthalpy value of 30.5 MJ/kg for both the 2.54-cm and 5.08-cm models, with a standard deviation of 3.6 and 4.1%, respectively.

For the frozen-flow case, q depends on the assumed surface catalytic recombination coefficient γ. For pure copper, Goulard estimated γ to be about 0.4 for oxygen recombination.[9] However, in the present test environment, visual inspection of the model surface after a test showed that the surface was discolored. According to Ref. 11, an "extremely slight" discoloration signifies oxidation of the surface, which changes the surface catalytic efficiency from that of copper to that of copper oxide.

Goulard estimated the γ for copper oxide to be 0.02 for oxygen recombination.[9] In Fig. 3, the predicted q values for a frozen flow are compared with the experimental data for γ of 0.4 and 0.02. As seen in Fig. 3, for $\gamma = 0.4$, the calculated q values are nearly those by the Fay–Riddell formula, and so the deduced H_c values are also those by the Fay–Riddell formula. For $\gamma = 0.02$, q is lower, and the deduced H_c values are higher: It is 37.1 MJ/kg by the 2.54-cm model and 35.0 MJ/kg by the 5.08-cm model.

The frozen-flow calculations shown in Fig. 3 were repeated with various values of γ, and the H_c values consistent with the measured values of q were determined. In Fig. 4, the enthalpy values deduced from different γ values are shown. One sees in Fig. 4 that the deduced H_c value is moderately sensitive to the γ value chosen. The true value of γ is unknown in the present experiment, partly because the extent of oxidation is unknown and partly because there is no information about the γ value for nitrogen recombination. In the present environment, the concentration of nitrogen atoms reaching the wall is at least three times that of oxygen atoms. In addition, nitrogen recombination produces nearly twice the energy of oxygen recombination per atom.

According to Fig. 4, if γ is zero, the deduced enthalpy will be over 100 MJ/kg. As will be shown hereafter, the enthalpy is deduced to be about 41 MJ/kg by the spectroscopic method. This enthalpy value would be consistent with the heat transfer rate data if γ were 0.01, as indicated in Fig. 4. In view of the uncertainty about the value of γ, especially for nitrogen recombination, such a low γ value should be considered to be well within the realm of possibilities.

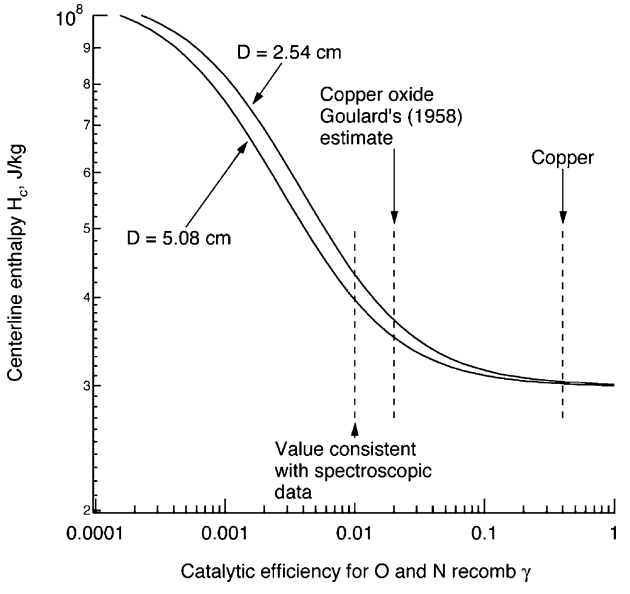

Fig. 4 Dependence of deduced centerline enthalpy H_c on assumed catalytic efficiency γ.

Spectrometric Method

Description of Method

The radiation emitted by the shock layer over the flat-faced calorimeters shown in Fig. 2 is observed by a spectrometer through a quartz lens and an optical fiber as shown schematically in Fig. 5. The solid angle of collection of the radiation was $f/635$. At the receiving focal plane, the collected radiation power is fed into an optical fiber 4 μm in diameter and 20 m in length. The output end of the optical fiber is connected to the entrance slit of a spectrometer. At the exit plane of this spectrometer, a one-dimensional photoelectric sensor array reads the spectrally resolved radiation power. The optical axis passes through a point 3.2 mm away from the model wall as shown in Fig. 5. The system measures radiation in the wavelength range from 380 to 900 nm, with a wavelength resolution (Gaussian full half width) of 4.5 nm.

A total of four spectra were obtained during this series of tests. All four spectra were nearly the same. The spectrum is shown in Fig. 6. The spectrum shows the emission from the N_2^+ first negative system, the N_2 first positive system, (possibly) CN violet, copper lines, and atomic nitrogen and oxygen lines. There are many lines of N and O that form the observed five groups of lines. Though it is irrelevant to the present work, the concentration of the copper vapor producing the observed intensity of the copper lines is calculated to be about 50 ppm by volume. Copper is believed to originate mostly from the electrodes.

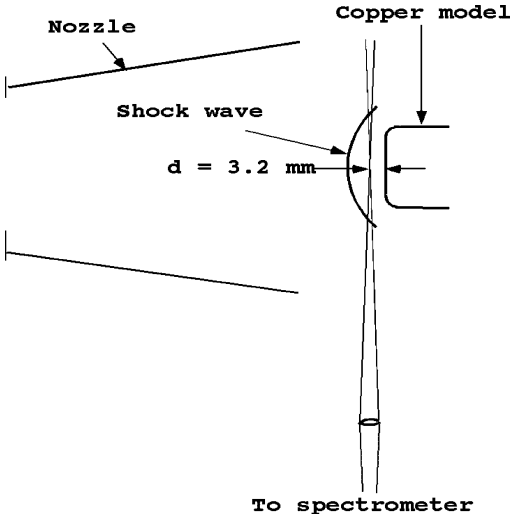

Fig. 5 Schematic of radiation emission measurement.

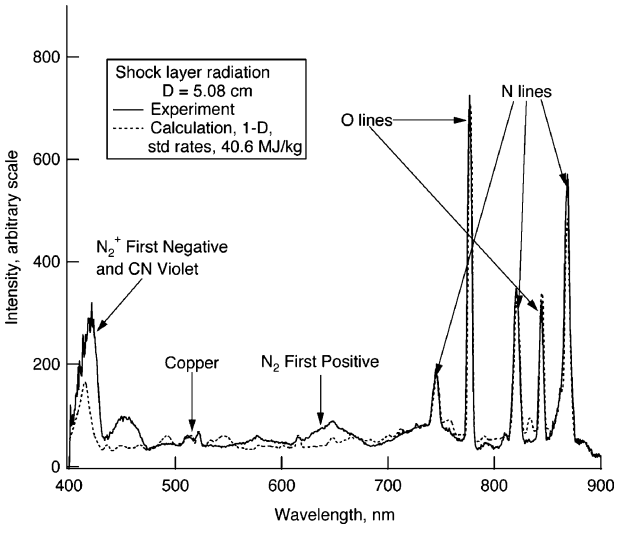

Fig. 6 Comparison between measured and calculated spectra of shock layer over copper calorimeter of 5.08-cm flat disk with rounded edge.

Theoretical spectra are then calculated assuming different values of flow enthalpy. The enthalpy value that numerically reproduces the measured spectrum is the desired enthalpy. Because the radiation emission occurs only in the core region of the flow, this procedure determines the core enthalpy H_c.

To calculate the theoretical spectrum, one must first determine the distribution of the thermodynamic properties in the shock layer. The shock-layer flowfield is determined in two ways: two dimensionally and one dimensionally. In the two-dimensional method, a CFD solution is obtained for the shock-layer flow assuming radial symmetry. The two-dimensional calculation is made for the nine different flow conditions: three enthalpy values (32, 39, and 47.3 MJ/kg in the settling chamber), and three sets of rate coefficient values mentioned earlier. The CFD calculation is performed using a simplified model for the determination of the vibrational–electron–electronic temperature in which the electronic excitation energy is neglected. A more accurate set of vibrational–electron–electronic temperature is obtained by performing a so-called ride-on calculation in which the conservation equations for the quantities of concern are integrated along the streamline already computed using the flow variables already computed. The quantities thus calculated are the concentrations of O^+ and N^+ and the vibrational–electron–electronic temperature.

In the one-dimensional method, the flowfield solution is obtained along the stagnation streamline using a viscous-shock-layer method. The body is assumed to be spherical, and the nose radius is chosen so that the shock standoff distance agrees with that obtained in the two-dimensional CFD calculation. The nose radius selected was 1.1 times that described in the section titled Heat Transfer Method, that is, 1.1 times 3.15 times the base radius of the tested model. The calculation is made for the four enthalpy values mentioned earlier. Only the standard rates were considered for the one-dimensional calculation. The vibrational–electron–electronic energy is calculated accounting for the electronic excitation energy. The flow condition is assumed to be uniform in the lateral direction (the direction parallel to the model surface) in the one-dimensional method.

From these solutions, a radiative transport calculation is made to determine the spectrum seen by the spectrometer using the latest version of the NEQAIR code.[12]

A problem arises in calculating the theoretical spectrum because the chromatic aberation of the lens, the finite dimension of the receiving surface of the optical fiber (4 μm), and the variation in the attenuation characteristics of the optical fiber on the incidence angle result in a blurring of the image of the focal point. To characterize the blurring phenomenon, one first defines the target plane, which is a plane normal to the optical axis and which passes through the central axis of the test section, as shown in Fig. 7.

In Fig. 7, the intersection of the optical axis and the target plane is the ideal focal point, that is, the focal point in the absence of blurring.

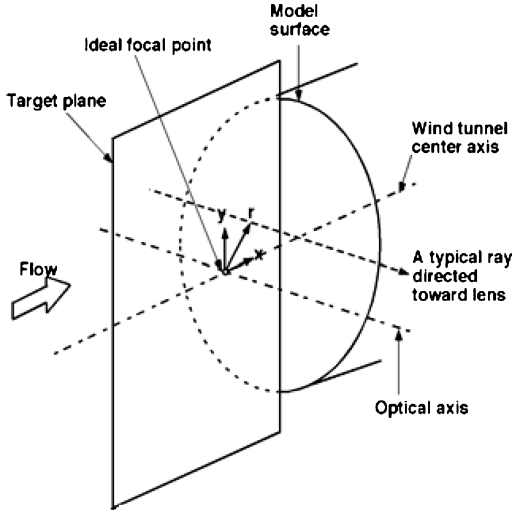

Fig. 7 Coordinate system related to definition of viewing function F.

Then one considers an arbitrary ray passing through the point x, y toward the lens as shown in Fig. 7. To calculate the contribution of this ray to the output of the spectrometer, one considers that a point light source is placed at that point in the target plane. The distance between the light source and the ideal focal point is $r = \sqrt{(x^2 + y^2)}$. One can define a viewing function $F(r)$, which is a relative sensitivity of the optical system. The function $F(r)$ is defined so that its areal integration is unity, that is,

$$2\pi \int_0^\infty F(r) r \, \mathrm{d}r = 1$$

This viewing function $F(r)$ was determined experimentally in Ref. 13 by placing a light source in the target plane, taking the readings on the spectrometer, and moving the light source to a different x location and repeating the measurement. The procedure found that $F(r)$ is a function of the wavelength λ and is expressible as

$$F(\lambda, r) = [a(\lambda)/\pi] \exp[-a(\lambda) r^2] \tag{3}$$

The coefficient $a(\lambda)$ is given in Ref. 13 at λ intervals from 25 to 50 nm. The value of the parameter $a(\lambda)$ is such that about 90% of the radiation power collected is from within a radius of 3 mm.

In principle, when the theoretical spectrum is calculated, the intensity of the radiation emanating from the shock layer along a specified ray should be multiplied by $F(\lambda, r)$. This resultant quantity is then integrated in both x and y directions. In reality, the double integration reduces to a single integration because the radiation emission from the gas is a function only of x and is independent of y: The integration in the y direction can be made analytically to give

$$f(\lambda, x) = 2 \int_0^\infty F(\lambda, r) \, \mathrm{d}y = \sqrt{\frac{a(\lambda)}{\pi}} \exp[-a(\lambda) x^2] \tag{4}$$

Thus, the calculated intensity emanating from the shock layer at the position x needs to be multiplied by $f(\lambda, x)$ and integrated only over x.

Results

The spectra calculated by the one-dimensional flow solution with four different assumed enthalpy values are shown in Fig. 8. The general features of the four spectra are substantially different. At low enthalpies, the molecular band structure is strong and atomic line radiation is very small; at high enthalpies, the atomic lines are strong and the molecular and radiation is very small. This trend is a result of the fact that the ratio of the atomic concentration to the concentration of N_2 increases rapidly as enthalpy increases in the range of concern.

The spectrum for the 40.6-MJ/kg case in Fig. 8 is compared with the experimental spectrum in Fig. 6. As seen, the theoretical

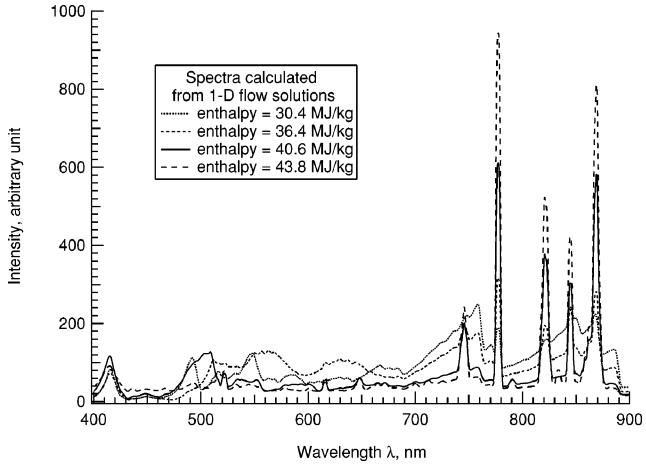

Fig. 8 Spectra calculated from one-dimensional flowfield solutions using standard rate coefficients for four different assumed enthalpy values.

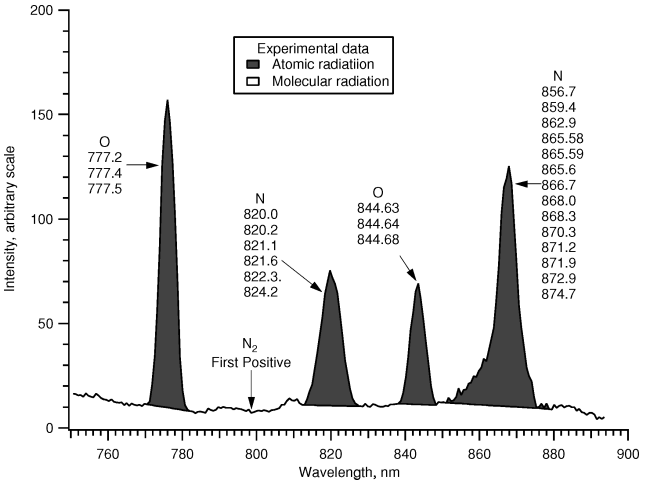

Fig. 9 Definition of atomic and molecular components in 750–900 nm region.

spectrum agrees fairly well with the experimental spectrum except in the region near 400 nm. The 400-nm region is dominated by the radiation from the N_2^+ and CN. The CN radiation originates from the carbonaceous impurities in the facility. Only a small concentration of carbon is needed to explain the observed relatively large radiation in the 400-nm region. No attempt is made to reconcile between the calculation and the experiment regarding CN. The nozzle flow properties for this 40.6-MJ/kg case were presented in Table 1 as the reference flow conditions.

Enthalpy is determined in the present work using the strong dependence of the atom-to-molecule concentration ratio on enthalpy. To do so, first the ratio of intensity of atomic radiation to that of molecular radiation is defined by integrating the area under the intensity curves from 750 to 900 nm, as shown in Fig. 9: The shaded area represents the intensity of atomic radiation and the unshaded area represents the intensity of molecular radiation. This method measures essentially the ratio of concentrations of atoms to molecules, that is, the degree of dissociation. As such, it is only weakly dependent on the local gas density: The density-dependent component of the energy is the thermal energy, which is relatively small in this highly dissociated regime. This wavelength range is the only wavelength range for air that presents this feature. The accuracy of this method is independent of the wavelength resolution of the spectrometer used because the area under the curve is independetn of the wavelength resolution. Noise is minimal: When the spectrometer is focused at points ahead of the bow shock, the received signal was less than 1% of that behind the bow shock.

The atomic-to-molecular radiation intensity ratios thus determined are compared in Fig. 10. In Fig. 10, the experimental value is shown with an estimated error bar of $\pm 10\%$. Both the one-dimensional and the two-dimensional theoretical values are shown. For the one-dimensional results, error bars are shown for an estimated error range of $\pm 40\%$, 20% in the uncertainty in the radiation intensity parameters plus 20% in the calculation of the nonequilibrium excited state populations. As seen, the intensity ratio is a very strong function of flow enthalpy. For the cases with the standard rates, the one-dimensional and two-dimensional calculations are approximately in agreement. The higher rates result in a higher ratios, and the lower rates results in lower ratios. However, the deviations of these nonstandard rates are relatively small.

According to Fig. 10, the observed atomic-to-molecular radiation intensity ratio is reproduced if the flow enthalpy were 40.6 MJ/kg by both the one-dimensional and two-dimensional methods assuming the standard rates. This supports the earlier assessment that this condition is the most likely flow condition as presented in Table 1. The 0.1 times the standard rates lead to an enthalpy value of 42 MJ/kg, whereas the 10 times the standard rates lead to 40 MJ/kg. Based on the larger of the deviations for the two, the uncertainty in the enthalpy value is determined to be 1.4 MJ/kg. The range of uncertainty

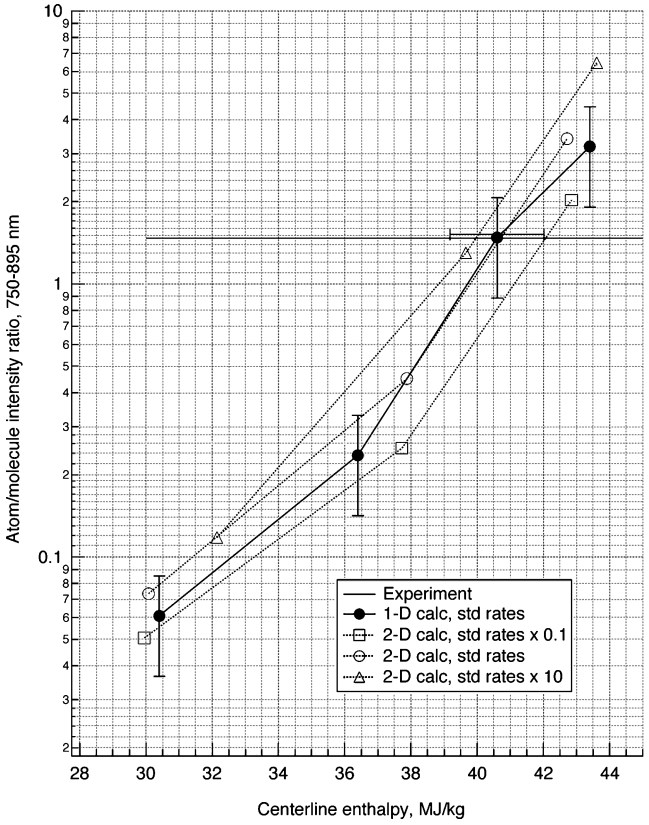

Fig. 10 Comparison of experimental and theoretical atomic-to-molecular intensity ratios.

of the enthalpy value is shown in Fig. 10 with a horizontal error bar around the one-dimensional value at 40.6 MJ/kg.

CFD Method

The CFD calculation of arc-jet flows was made first in Ref. 14. The code developed therein was found not be suitable for the present operating condition. An improved version of the CFD code has been developed at NASA Ames Research Center as reported in Refs. 15 and 16. In the new version, the latest version of the radiation parameters described in Ref. 17 is used, which includes the latest available information on atomic radiation and five molecular band systems of N_2 in the vacuum UV wavelength range. A three-band model was constructed using this radiation database. The introduction of argon in the upstream electrode chamber is accounted for, and airflow is assumed to be introduced radially inward from the constrictor wall. Equilibrium is assumed everywhere in the calculated domain, that is, to points slightly past the throat. The downstream boundary condition is given at a point past the nozzle throat. The code requires only the mass flow rate and electrical current input to be specified. Details of the method are described in Refs. 15 and 16.

The flow conditions calculated by this method are shown for the nozzle throat in Figs. 11a and 11b. The mass flow rate for this calculation was 0.411 kg/s, and the electrical current and voltage were 6066 A and 4608 V, respectively, resulting in a power input of 28.4 MW. Calculated efficiency was 0.386. The mass-averaged enthalpy was calculated to be 27.0 MJ/kg, which is lower than the values determined through the energy balance and the sonic throat method by 6.6%. The centerline enthalpy was calculated to be 41.0 MJ/kg, in close agreement (within 1%) with the value determined spectroscopically. The centerline-to-average enthalpy ratio was $41.0/27.0 = 1.52$. If this centerline enthalpy value is used in the calculation of the stagnation-point heat transfer rate for the copper calorimeter, the calculated rates agree with the measured values under the assumption that the catalytic efficiency is 0.02.

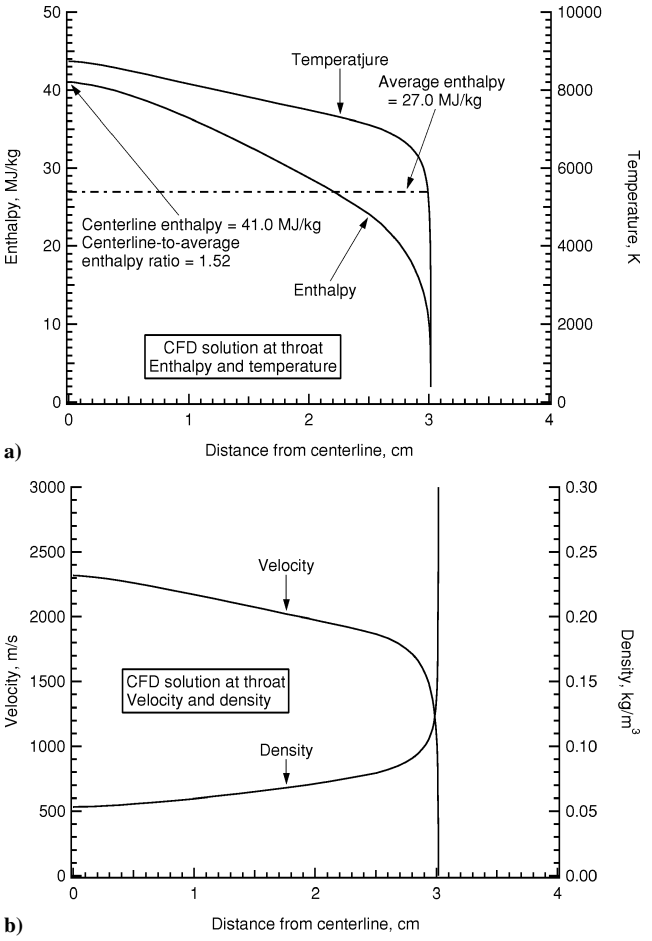

Fig. 11 Results of CFD calculation at nozzle throat: a) enthalpy and temperature and b) velocity and density.

Discussion

In Fig. 12, the results from the five methods are summarized and compared. The mean value of the mass-averaged enthalpy between the heat balance method and the sonic throat method is 28.8 MJ/kg, as compared to the CFD value of 27.0 MJ/kg. The heat transfer rate method yields a minimum value of the centerline enthalpy of 30.5 MJ/kg. The spectrometric method yields the centerline enthalpy value of about 40.6 MJ/kg, as compared to the CFD value of 41.0 MJ/kg.

Based on the spectrometrically determined centerline enthalpy value, the ratio of the centerline-to-average enthalpies is

$$\frac{\text{centerline enthalpy}}{\text{average enthalpy}} = \frac{40.6}{28.8} = 1.41$$

The CFD value of this ratio, 1.52, is only slightly different from this value. That the centerline enthalpy is higher than the average by 40 or 50% is reasonable. All six methods considered in the present work seem to function as well as expected, and no contradictions are found among them. The good agreement between the spectroscopic method and the CFD calculation on the centerline enthalpy lends credence to the centerline value obtained. In the future, in the absence of an independent measurement of centerline enthalpy, it could be estimated approximately from the average value using the centerline-to-average enthalpy ratio obtained in the present work, provided that the operating condition is similar to the present one.

The centerline enthalpy value of 40.6 MJ/kg corresponds to the flight velocity of 9.0 km/s. The combination of the enthalpy and the pitot pressure of the present test corresponds to a flight altitude of 52 km.

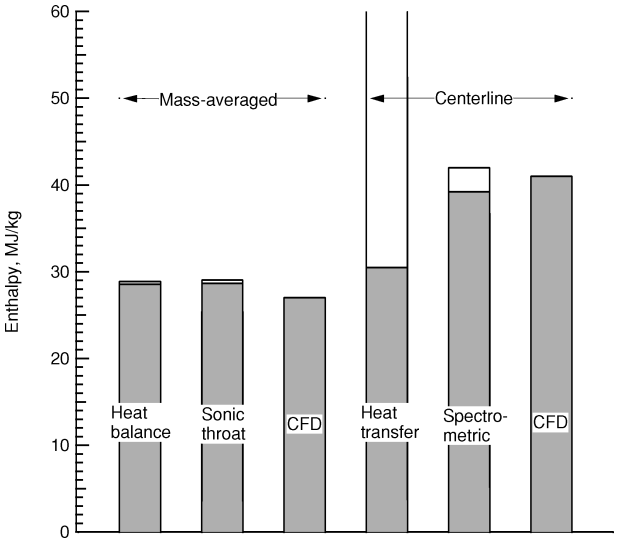

Fig. 12 Comparison of enthalpy values.

Conclusions

For one selected operating condition of the IHF at NASA Ames Research Center, the heat balance method yields a mass-averaged enthalpy of 28.7 ± 0.5 MJ/kg, whereas the sonic throat method yields 28.8 ± 0.5 MJ/kg. The lower bound of the centernline enthalpy as determined by the heat transfer rate to the stagnation point of a blunt body, corresponding to an equilibrium flow or a frozen flow for a fully catalytic wall, is 30.5 ± 1.2 MJ/kg. When the spectrum of the radiation emitted by the shock layer over the blunt body is analyzed, the centerline enthalpy is determined to be 40.6 ± 1.4 MJ/kg. Based on the spectral data, the ratio of the centerline to average enthalpies is about 1.41. The CFD calculation yields a centerline enthalpy value that closely (within 1%) agrees with the spectrometric value, as well as an average enthalpy value only slightly (6.6%) lower than the measured values. Thus, all methods are consistent with the average enthalpy value of about 29 MJ/kg and the centerline enthalpy value of about 41 MJ/kg.

Acknowledgments

The first author wishes to acknowledge the support provided by NASA Ames Research Center through Contract NAS2-99092 to Eloret Corporation. The authors express their sincere thanks to Eric Sarabia for carrying out the tests in the arc-jet facility.

References

[1]Grinstead, J. H., Driver, D. M., and Raiche, G. A., II, "Radial Profiles of Arc-Jet Flow Properties Measured with Laser-Induced Fluorescence of Atomic Nitrogen," AIAA Paper 2003-0400, Jan. 2003.

[2]Park, C., and Lee, S. H., "Validation of Multitemperature Nozzle Flow Code," *Journal of Thermophysics and Heat Transfer*, Vol. 9, No. 1, 1995, pp. 9–16.

[3]Park, C., *Nonequilibrium Hypersonic Aerothermodynamics*, Wiley, New York, 1990, p. 326.

[4]Hightower, T. M., Balboni, J. A., MacDonald, C. L., Anderson, K. F., and Martinez, E. R., "Enthalpy by Energy Balance for Aerodynamic Heating Facility at NASA Ames Research Center Arc Jet Complex," ISA TP02-AERO-2000 Instrumention, Systems, and Automation Society, San Diego, CA, May 2002.

[5]Winovich, W. "On the Equilibrium Sonic-Flow Method for Evaluating Electric-Arc Air-Heater Performance," NASA TN D-2132, March 1964.

[6]Shephard, C., Milos, F., and Taunk, J., "A Sonic Flow Equation for Electric Arc Jets," AIAA Paper 93-3183, July 1993.

[7]Zoby, E. V., and Sullivan, E. M., "Effects of Corner Radius on Stagnation Point Velocity Gradients on Blunt Axisymmetric Bodies," NASA TM X-1067, March 1965.

[8]Fay, J. A., and Riddell, F. R., "Theory of Stagnation Point Heat Transfer in Dissociated Air," *Journal of the Aeronautical Sciences*, Vol. 25, No. 2, 1958, pp. 73–121.

[9]Goulard, R., "On Catalytic Recombination Rates in Hypersonic Stagnation Heat Transfer," *Jet Propulsion*, Vol. 28, No. 11, 1958, pp. 737–745.

[10]Zoby, E. V., "Empirical Stagnation-Point Heat-Transfer Relation in Several Gas Mixtures at High Enthalpy Levels," NASA TN D-4799, Oct. 1968.

[11]Winkler, E. L., and Sheldahl, R. E., "Influence of Calorimeter Surface Treatment on Heat-Transfer Measurements in Arc-Heated Test Streams," *AIAA Journal*, Vol. 4, No. 4, 1966, pp. 715–716.

[12]Whiting, E. E., Park, C., Liu, Y., Arnold, J. O., and Paterson, J. A., "NEQAIR96, Nonequilibrium and Equilibrium Radiative Transport and Spectra Program: User's Manual," NASA Reference Publ. 1389, Dec. 1996.

[13]Raiche, G. A., II, and Driver, D. M., "Shock Layer Optical Attenuation and Emission Spectoscopy Measurements During Arc Jet Testing with Ablating Models," AIAA Paper 2004-0825, Jan. 2004.

[14]Kim, K. H., Rho, O. H., and Park, C., "Navier–Stokes Computation of Flows in Arc Heaters," *Journal of Thermophysics and Heat Transfer*, Vol. 14. No. 2, 2000, pp. 250–258.

[15]Sakai, T., and Olejniczak, J., "Navier–Stokes Computations for Arc-Jet Flows," AIAA Paper 2001-3014, June 2001.

[16]Sakai, T., and Olejniczak, J., "Improvments in a Navier–Stokes Code for Arc Heater Flows," AIAA Paper 2003-3782, June 2003.

[17]Park, C., "Stagnation-Point Radiation for Apollo 4," *Journal of Thermophysics and Heat Transfer*, Vol. 18, No. 3, 2004, pp. 349–357.